# Peripapillary Scleral Bowing Increases with Age and Is Inversely Associated with Peripapillary Choroidal Thickness in Healthy Eyes

YA XING WANG, HONGLI YANG, HAOMIN LUO, SEUNG WOO HONG, STUART K. GARDINER,
JIN WOOK JEOUNG, CHRISTY HARDIN, GLEN P. SHARPE, KOUROS NOURI-MAHDAVI, JOSEPH CAPRIOLI,
SHABAN DEMIREL, CHRISTOPHER A. GIRKIN, JEFFREY M. LIEBMANN, CHRISTIAN Y. MARDIN,
HARRY A. QUIGLEY, ALEXANDER F. SCHEUERLE, BRAD FORTUNE, BALWANTRAY C. CHAUHAN, AND
CLAUDE F. BURGOYNE

• PURPOSE: To use optical coherence tomography (OCT) to 3-dimensionally characterize the optic nerve head (ONH) in peripapillary scleral bowing in non-highly myopic healthy eyes.

• DESIGN: Cross-sectional, multicenter study.

• METHODS: A total of 362 non-highly myopic ($+6$ diopters [D] $>$ spherical equivalent $> -6D$) eyes of 362 healthy subjects from 20-90 years old underwent OCT ONH radial B-scan imaging. Bruch's membrane (BM), BM opening (BMO), anterior scleral canal opening (ASCO), and the peripapillary scleral surface were segmented. BMO and ASCO planes were fit, and their centroids, major axes, ovality, areas and offsets were determined. Peripapillary scleral bowing was characterized by 2 parameters: peripapillary scleral slope (ppSS) of 3 anterior peripapillary scleral segments (0-300, 300-700, and 700-1,000 μm from the ASCO centroid); and ASCO depth relative to a peripapillary scleral reference plane (ASCOD-ppScleral). Peripapillary choroidal thickness (ppCT) was calculated relative to the ASCO as the minimum distance between the anterior scleral surface and BM.

• RESULTS: Both ppSS and ASCOD-ppScleral ranged from slightly inward through profoundly outward in direction. Both parameters increased with age and were independently associated with decreased ppCT.

• CONCLUSIONS: In non-highly myopic healthy eyes, outward peripapillary scleral bowing achieved substantial levels, was markedly increased with age, and was independently associated with decreased peripapillary choroidal thickness. These findings provide a normative foundation for characterizing this anatomy in cases of high myopia and glaucoma and in eyes with optic disc tilt, torsion, and peripapillary atrophy. (Am J Ophthalmol 2020;217:91–103. © 2020 Elsevier Inc. All rights reserved.)

THE TERM "NEURAL CANAL" IS USED TO REFER TO THE optic nerve head (ONH) connective tissue pathway that the retinal ganglion cell axons pass through on their way to achieve the orbital optic nerve.[1,2] The neural canal extends from Bruch's membrane opening (BMO) through the anterior and posterior scleral canal openings (Figure 1). The authors proposed that the offset of the anterior scleral canal opening (ASCO) relative to the BMO (ASCO/BMO offset) was used to determine the direction, obliqueness, and minimum cross-sectional area of the neural canal.[1] Hypothetically that temporal displacement of BMO relative to the ASCO and outward bowing of the peripapillary sclera bowing fundamentally underlie the phenotype of the ONH tissues in non-highly myopic and highly myopic eyes and that both of them contribute to a given ONH susceptibility to developing peripapillary atrophy and/or glaucomatous damage at all levels of intraocular pressure (IOP) including those that are considered statistically normal.
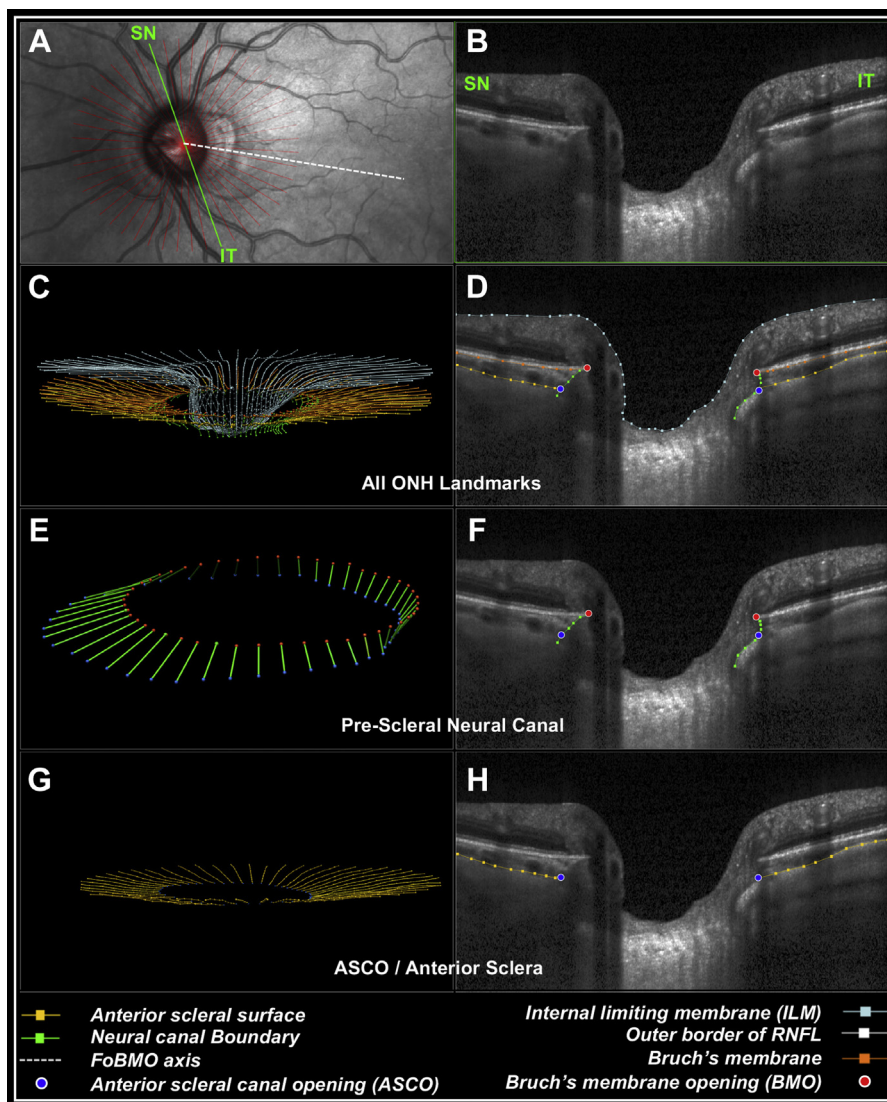
**FIGURE 1.** OCT anatomic landmarks. (A) A 24-radial B-scan OCT data set is shown (red lines) relative to the FoBMO centroid axis (white dotted line). The single green line depicts the representative B-scan shown in (B) superior nasal (SN) left and inferior-temporal (IT) right. (C) The 3D point cloud of all segmented OCT landmark points, which are segmented in B-scan in (D). (E) The prescleral neural canal point cloud extends from BMO (red dots), along the neural canal boundary to the ASCO, as shown within an individual B-scan in (F). (G) The ASCO (blue dots) and anterior scleral canal surface (yellow squares) point cloud which is shown within an individual B-scan in (H) (see Methods for a detailed description of this anatomy and its segmentation). ASCO = anterior scleral canal opening; BMO = Bruch's membrane opening; FoBMO = fovea-to-BMO distance; OCT = optical coherence tomography.

An increase in peripapillary scleral bowing with age was recently reported[3] in 619 elderly (mean 60-year-old) Chinese subjects using a single horizontal B-scan in which a "peripapillary scleral angle" was estimated by projecting lines parallel to the nasal and temporal anterior peripapillary scleral surfaces and measuring the angle of their intersection. By the conventions of that study, if those lines intersected in an upright "V"-shaped peripapillary scleral, bowing was positive (outward) in direction, and if the "V" was inverted, it was negative (inward) in direction. The elderly eyes in that study predominantly demonstrated outward peripapillary scleral bowing, and even within this constrained age range, outward bowing significantly increased with age and was significantly associated with peripapillary choroidal thinning.[3]

The fact that peripapillary scleral bowing increased with age and was associated with peripapillary choroidal thinning in that study,[3] suggests that peripapillary scleral bowing may mechanistically contribute to the increase in the prevalence of peripapillary atrophy with age[4–8] and in glaucoma.[5,9,10] Studies by the present authors[11,12] and others[13–21] have emphasized the biomechanical links among the
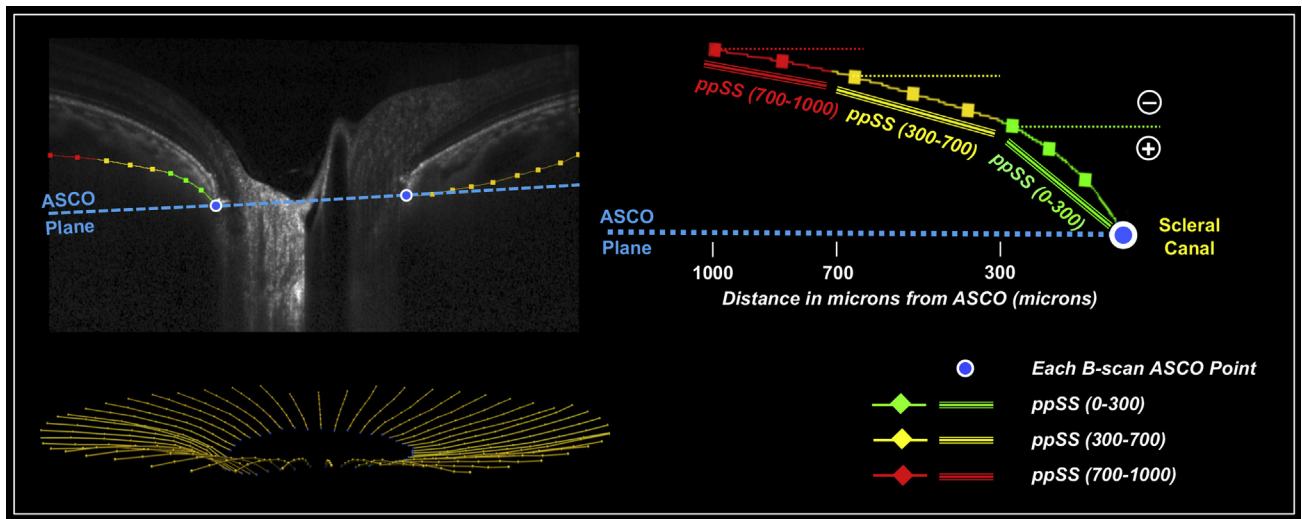
**FIGURE 2.** ppSS measured in 3 anterior ppScleral segments (relative to the distal position of each segment) within each B-scan. The peripapillary anterior sclera surface was fitted using a trilinear model, and ppSS was calculated for 3 juxtacanalicular anterior scleral segments (0-300 μm, 300-700 μm, and 700-1,000 μm) measured relative to the ASCO within the ASCO reference plane after projection of these measurement points onto the anterior scleral surface. Within each B-scan, the slope direction for each anterior scleral segment was determined by the position of its proximal measurement point relative to its distal measurement point. By convention, "inward" peripapillary scleral bowing occurred when the proximal end of a segment was "above" the distal end and its sign was defined to be negative (−). "Outward" peripapillary scleral bowing was occurred when the proximal end of a segment was "below" its distal end and its sign was defined as positive (+). ppSS was multiplied by 100 for presentation and analysis. Note that, because slope is unitless, ppSS is a unitless parameter. ASCO = anterior scleral canal opening; ppSS = peripapillary scleral slope.

peripapillary sclera, the dural sheath insertion,[2,22,23] the laminar beam insertions, and the small penetrating branches of the posterior ciliary arteries that supply the juxtacanalicular choroid and laminar beams.[24] Hayreh and associates[25] demonstrated that this blood supply was preferentially susceptible to acute IOP elevation and hypothesized that compromise of this blood supply contributed to a primary vascular insult in glaucoma and the frequent presence of peripapillary choroidal atrophy in aging and glaucoma.[26]

The purpose of the present study was to use optical coherence tomography (OCT) imaging to 3-dimensionally (3D) characterize peripapillary scleral bowing in non-highly myopic healthy eyes by using 2 parameters, one parameter based on the slope of the peripapillary sclera (peripapillary scleral slope [ppSS]), and the other parameter based on the depth of ASCO relative to a peripapillary reference plane (ASCO depth relative to a peripapillary scleral reference plane [ASCOD-ppScleral]). The association of each parameter was then determined with ocular and demographic factors such as age, axial length, and peripapillary choroidal thickness (ppCT).[27]

## SUBJECTS AND METHODS

• **CONVENTIONS:** The term ONH is used to refer to the tissues that are contained within the scleral canal and those immediately adjacent to it (i.e., the peripapillary sclera,

choroid, and retina and the immediate retrolaminar optic nerve). In this report OCT parameters are italicized to distinguish the parameters from the morphologic relationships they measure.

• **PARTICIPANTS:** A total of 362 healthy individuals were recruited from 8 centers (5 in the United States, 2 in Germany, and 1 in Canada).[1,27–29] Among these participants were 246 self-identified European descendants, 47 ethnic Hispanics, 47 African descendants, 19 Asian descendants, and 3 Native American descendant. Approximately equal numbers of subjects were recruited in each decade group from 20 to 90 years. At the first visit, a medical and ophthalmic history were obtained, followed by intraocular pressure (IOP) measurement, anterior segment and external eye examinations, Van Herrick angle assessment, standard Snellen or Early Treatment Diabetic Retinopathy Study visual acuity, refraction, central keratometry, and axial length assessments. Standard automated perimetry (Humphrey 24-2 Swedish interactive thresholding algorithm; Carl Zeiss Meditec, Dublin, California) was repeated once if deemed unreliable or outside normal limits. OCT imaging, ophthalmoscopic examination of the posterior pole, and stereo photography were followed by Goldmann applanation tonometry and pachymetry.

All test procedures were performed on both eyes of each participant, but only 1 eye was randomly selected for analysis. Participants were recruited to represent the ethnic
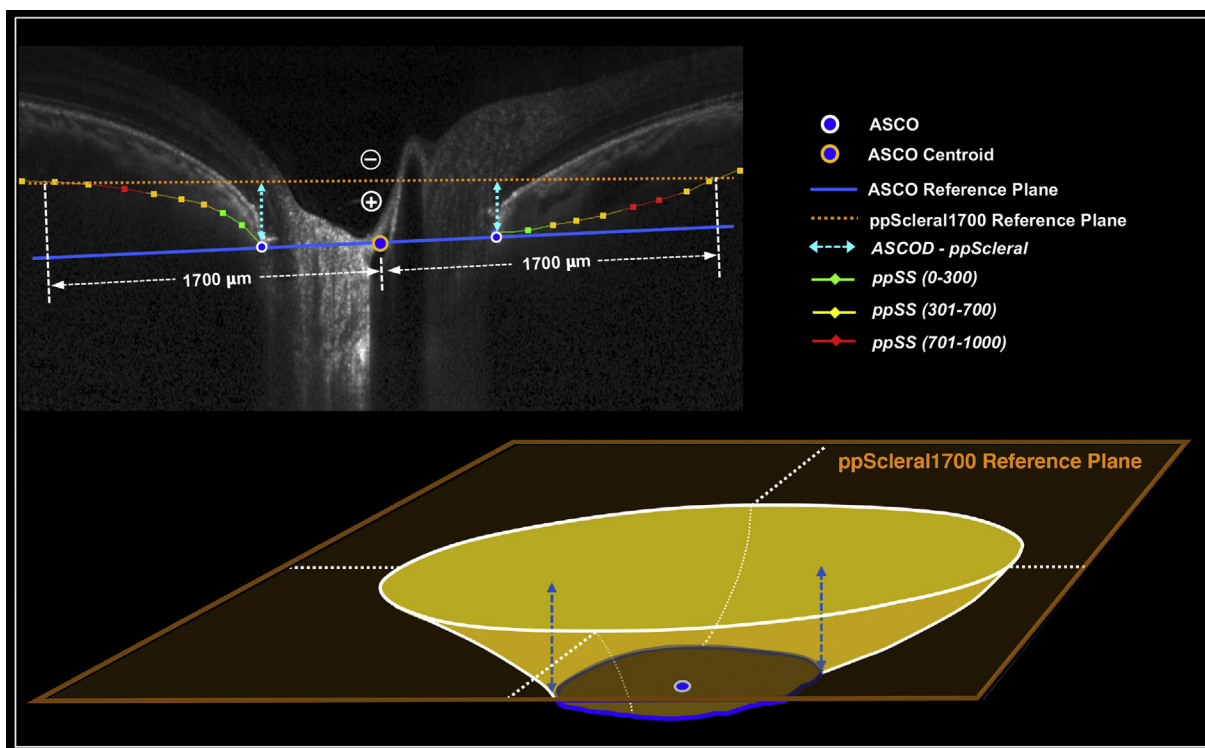
FIGURE 3. *ASCOD-ppScleral* in 2D (above) and in 3D (below). A 1,700-μm peripapillary scleral reference plane was defined by the plane that best fit the anterior scleral surface points at a distance 1,700 μm from the ASCO centroid (measured within the ASCO reference plane). ASCOD was defined at each ASCO point as the minimum distance to the ppScleral reference plane (negative [−] when above the plane and positive [+] when below). Global *ASCOD-ppScleral* was defined as the average of 48 individual ASCO point depth values. Sectoral *ASCOD-ppScleral* was calculated as the average depth value of the 4 ASCO points within each sector (24 radial B-scans, each containing 2 ASCO points, yielded 48 ASCO measurement points distributed over 12 30-degree FoBMO sectors). 2D/3D = 2 dimensional/3 dimensional; *ASCOD-ppScleral* = anterior scleral canal opening depth relative to a 1,700-μm peripapillary scleral reference plane; FoBMO = fovea-to- Bruch's membrane opening.

composition of the US population[30] as mandated by the US Food and Drug Administration. The study adhered to tenets of the Declaration of Helsinki for research involving human participants and was approved by the institutional review board of each participating institution. Each participant provided signed informed consent.

Inclusion criteria included: 1) age between 18 and 90 years old; 2) clinically normal eye examination results without clinically significant vitreoretinal or choroidal disease and prior intraocular surgery, except for cataract or refractive surgery; 3) IOP of 21 mm Hg or less; 4) best-corrected visual acuity of 20/40 or better; 5) refractive error within 6 diopters (D) spherical error and 2D astigmatic error; and 6) normal visual field using the glaucoma hemifield test and mean deviation within normal limits. Subjects were excluded if any of the following were found: 1) history of glaucoma; 2) ONH photographs of insufficient quality; 3) OCT images of insufficient quality (see below); or 4) unreliable visual field results.

• OCT IMAGE ACQUISITION AND SEGMENTATION: The ONH, peripapillary retinal nerve fiber layer and macula were imaged with spectral domain OCT (Spectralis model; Heidelberg Engineering GmbH, Heidelberg, Germany; with Heyex version 1.9.10.0 software). Prior to image acquisition, refractive correction and keratometry values were entered into the system software. The operator then manually identified and marked the fovea in a live B-scan, then centered the imaging field on the ONH, where the 2 BMO points in each of 2 perpendicular ONH radial B-scans were identified. These steps established the eye-specific, fovea-BMO (FoBMO) axis, which was used as the reference for the acquisition of all OCT B-scans (Figure 1).[31–33] The complete ONH imaging pattern consisted of 24 radial B-scans (15-degrees apart with each B-scan containing 768 A-scans) centered on the BMO and acquired in enhanced depth imaging mode[34] with an average of 25 repetitions each. Raw OCT volumes were exported from the device and imported into custom 3D visualization and segmentation software (ATL 3D Suite).[35] ONH and peripapillary landmarks were manually segmented[1,27,28] in each radial B-scan and then reconstructed in 3D (Figure 1). Segmented landmarks included the internal limiting membrane, posterior surface of the

**TABLE 1.** Demographic and Ocular Characteristics of the Participants

| | All Subjects | European Descent | Hispanic Descent | African Descent | Asian/Native American Descent[a] | ANOVA or Chi-Squared Test[b] |
|---|---|---|---|---|---|---|
| | n = 362 | n = 248 | n = 47 | n = 47 | n = 22 | |
| Females | 202 (56%) | 137 (56%) | 30 (64%) | 22 (47%) | 13 (59%) | 0.41 |
| Left Eye | 181 (50%) | 123 (51%) | 25 (51%) | 25 (53%) | 9 (41%) | 0.83 |
| age, y | 50.6 (17.5) | 52.2 (18.3) | 45.3 (14.1) | 49.4 (14.8) | 47.3 (19.3) | 0.06 |
| axial length, mm | 23.7 (1.0) | 23.7 (0.9) | 23.9 (1.0) | 23.8 (1.0) | 24.1 (1.1) | 0.18 |
| IOP, mm Hg | 15.0 (3.0) | 14.6 (2.7) | 14.3 (2.7) | 14.9 (2.7) | 14.0 (2.5) | 0.49 |
| CCT, μm | 555 (33) | 555 (35) | 556 (26) | 546 (29) | 573 (22) | **0.012** |
| SE, D | −0.47 (1.8) | −0.3 (1.7) | −0.4 (1.9) | −0.8 (1.8) | −1.93 (2.1) | **< 0.001** |

CCT = central corneal thickness; D = diopter; IOP = intraocular pressure; SE = spherical equivalent.

Values are n (%) or mean (±SD). *P*-values <0.05 were given in bold.

[a]n = 19 (5.2%) Asian and n = 3 (0.8%) Native American.

[b]ANOVA or Chi-square test to assess for the significance of the effect of ethnicity.

**TABLE 2.** Global peripapillary scleral bowing parameters overall.

| Peripapillary Scleral Bowing | Mean (±SD) | Range |
|---|---|---|
| ppSS | | |
| ppSS (0-300) | 3.4 (4.8) | −7.7 to 25.9 |
| ppSS (300-700) | 2.6 (4.4) | −8.3 to 31.4 |
| ppSS (700-1000) | 2.9 (4.3) | −6.8 to 30.6 |
| *ASCOD*-ppScleral (μm) | 25.2 (35.2) | −39.8 to 245.6 |

ASCO = anterior sclera canal opening; *ASCOD*-ppScleral = anterior sclera canal opening depth relative to a peripapillary scleral reference plane; ppSS = peripapillary scleral slope; SD = standard deviation.

Note that, because the slope is unitless, ppSS is a unitless parameter. Note also that ppSS is measured between 4 points, measured from the ASCO: ASCO 0 μm, 300 μm, 700 μm, and 1,000 μm.

Bruch's membrane/retinal pigment epithelium complex, BMO, neural canal wall, anterior scleral surface, and the ASCO (segmented on each side of the canal by visually projecting the plane of the peripapillary anterior scleral surface through the neural canal wall and marking their intersection).[1,27,28] All manual segmentations were performed by trained observers in the Optic Nerve Head Research Laboratory, Devers Eye Institute.

• OCT PARAMETERS ACCORDING TO ONH MORPHOLOGY: Quantification of all parameters was performed using MATLAB version 9.0.0.341360 software (MathWorks, Natick, Massachusetts). All left eye data were converted to right eye format. For each eye, separate ellipses and planes were fitted to the 48 segmented BMO and 48 segmented ASCO points, each satisfying a least mean square error restraint. The anterior scleral surface points were interpolated using B-splines (Figure 1G). Based on the BMO fitted ellipse, a BMO centroid, area, and ovality index (ellipse major axis/ellipse minor axis) were calculated.[36] An ASCO centroid, area, and ovality index were similarly calculated.

To characterize peripapillary scleral bowing, 2 OCT parameters, peripapillary scleral slope (ppSS) and an *ASCOD-ppScleral* using a depth relative to a 1,700-μm peripapillary scleral reference plane were used. For both parameters, by convention, "inward" peripapillary scleral bowing was defined as negative in direction, and "outward" peripapillary scleral bowing was defined as positive in direction (Figures 2 and 3). Because positive and negative sectoral values for both parameters cancelled one another when considered globally, sectoral ppSS and sectoral *ASCOD-ppScleral* are emphasized.

• PPSS: The anterior peripapillary scleral surface in each B-scan was fitted with a 3-segment linear model implemented with a nonlinear curve-fitting function, the LSQCURVEFIT application in Matlab version 7.3.0.267 (MathWorks), which minimized the least square error between fitted and raw values. Three peripapillary scleral segments (0-300 μm, 300-700 μm, and 700-1,000 μm), were measured relative to each ASCO point within the ASCO reference plane and projected to the anterior scleral surface (Figure 2). Within each B-scan, the slope sign (direction) for each segment was defined relative to a plane (parallel to the ASCO reference plane) through its most distal point. For each segment, the segmental slope was positive (outward bowing) when the proximal segmental point was below the distal segment point and negative (inward bowing) when the proximal segment point was above the distal segment point. Sectoral slope values
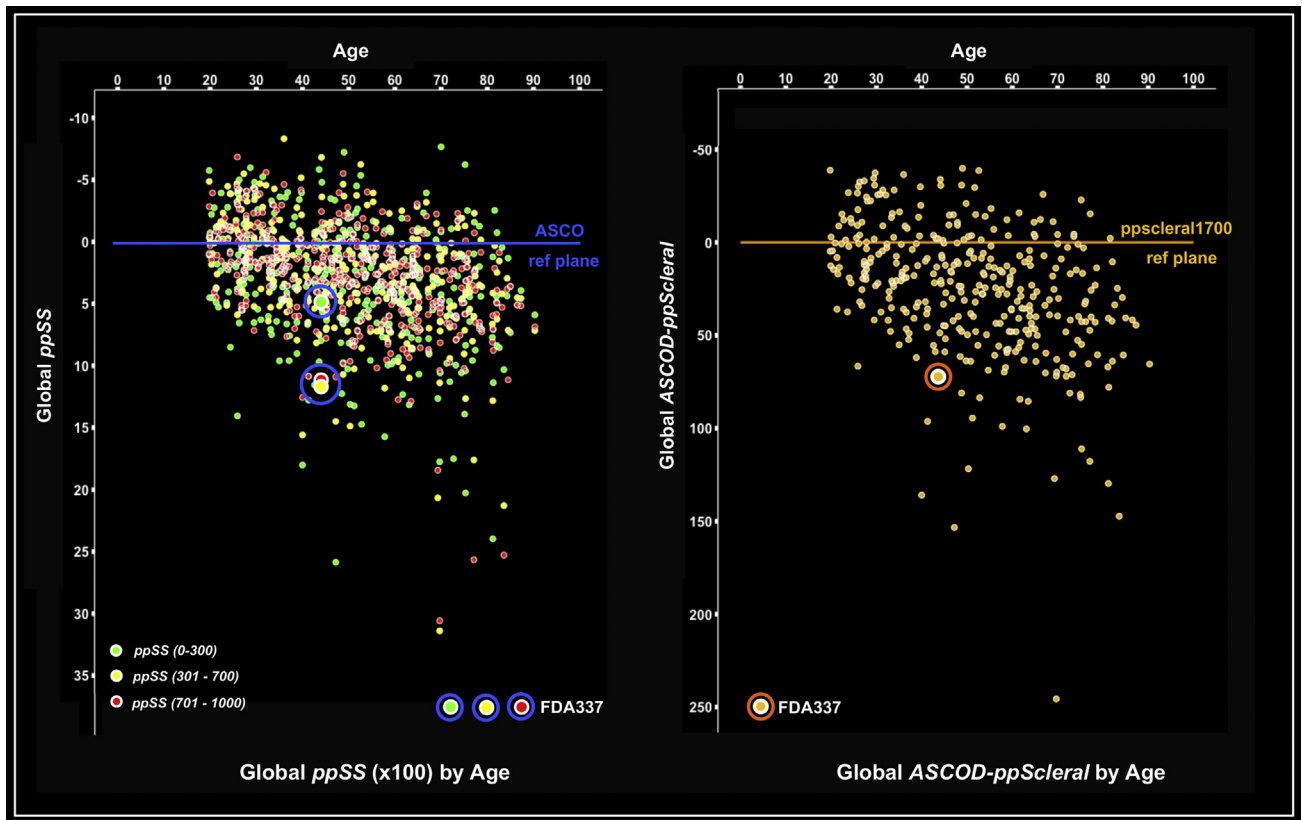
**FIGURE 4.** Distribution of global ppSS (for each ASCO segment) (left) and global *ASCOD-ppScleral* (right) by age. By convention, for both parameters, "inward" peripapillary scleral bowing is defined as negative (upward) in direction and an "outward" peripapillary scleral bowing is defined as positive (downward) in direction. (Left) Global data for each ppSS segment (0-300 μm, 300-700 μm, and 700-1,000 μm [color-coded]) for each study eye are plotted. (Right) A single global *ASCOD-ppScleral* value is plotted for each study eye. For both parameters, the data for the representative study eye shown in Figure 7 (FDA337) are highlighted. *ASCOD-ppScleral* = anterior scleral canal opening depth relative to a 1,700-μm peripapillary scleral reference plane; ppSS = peripapillary scleral slope.

for each anterior scleral segment were calculated as the average slope value of the 4 B-scans within each sector. Global ppSS values for each segment were calculated as the mean of the 48 B-scan slope values per segment. Slope data were multiplied by 100 for presentation and analysis.

- **ASCOD-PPSCLERAL:** *ASCOD-ppScleral* was used to measure the depth of the ASCO relative to a peripheral scleral reference plane (Figure 3) created by fitting a plane to 48 anterior scleral surface points located 1,700 μm from the ASCO centroid within each radial B-scan (MATLAB version 7.3.0.267). *ASCOD-ppScleral* was determined at each segmented ASCO point as the minimum distance to the peripapillary scleral reference plane (negative when above the plane and positive when below). *ASCOD-ppScleral* was defined sectorally as the average depth value of the 4 ASCO points within each 30-degree sector and globally as the average value of all 48 ASCO measurement points.

- **OTHER OCT PARAMETERS:** In order to assess their associations with the primary OCT parameters of this study, the following previously reported[1,27–29] parameters were generated as briefly described below.

The ASCO/BMO offset magnitude, neural canal direction, neural canal obliqueness, and neural canal minimum cross-sectional area (NCMCA).[1] ASCO/BMO offset magnitude was defined by projecting the ASCO/BMO centroid vector (the vector connecting the BMO and ASCO centroids, also called the neural canal axis vector) to the BMO reference plane and measuring the length of its projection. Neural canal obliqueness was defined by the angle between the ASCO/BMO centroid vector and the BMO centroid vector (a vector perpendicular to the BMO plane that passes through the BMO centroid).

- **PERIPAPILLARY CHOROIDAL THICKNESS:** Global and 30-degree sectoral ppCT[27] measurements were generated as the minimum distance between the anterior scleral surface and Bruch's membrane at 100, 300, 500, 700, 900, and 1,100 μm from the ASCO.
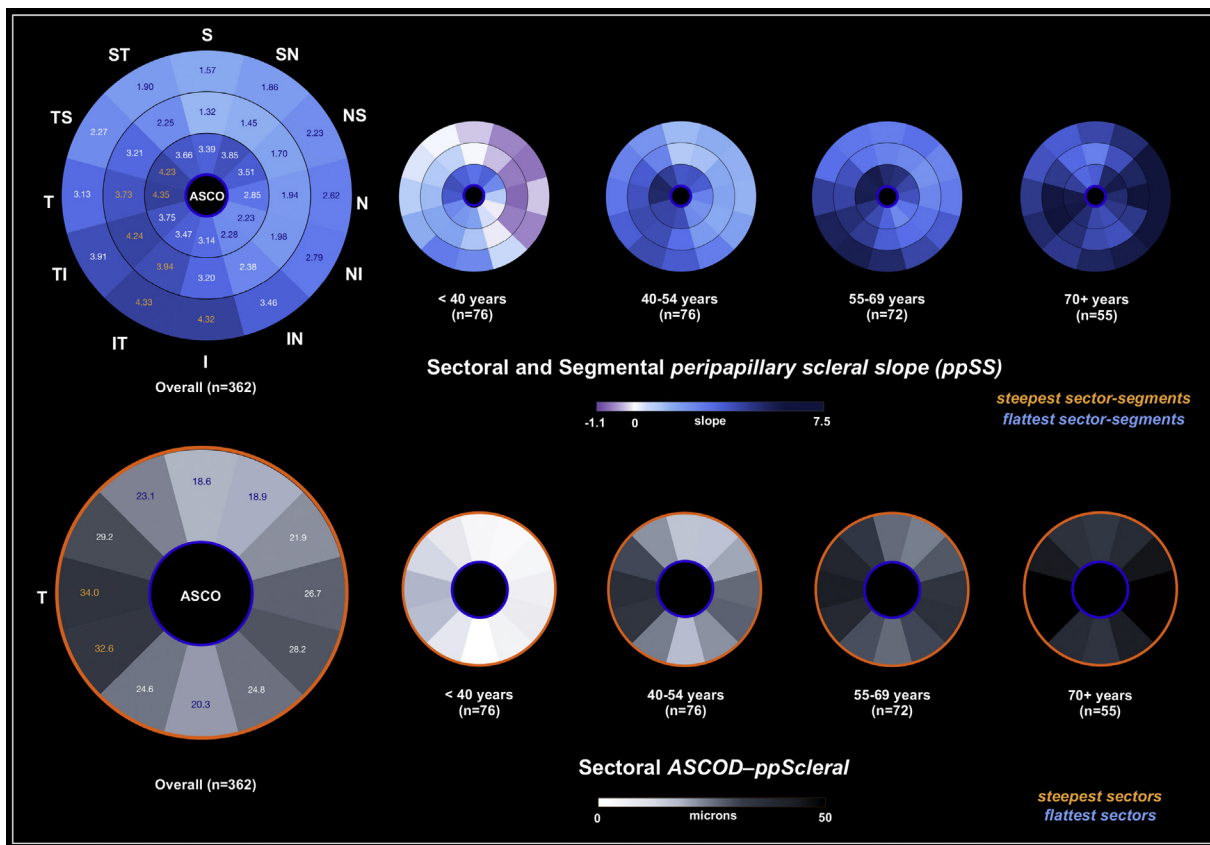
FIGURE 5. Peripapillary scleral bowing as characterized by sectoral ppSS (above) and sectoral ASCO depth relative to a peripapillary scleral reference plane (ASCOD-ppScleral) (below). Data are shown overall and by age group. The upper ppSS plots depict ppSS (0-300 μm) segment data (inner ring), ppSS (300-700 μm) segment data (middle ring), and ppSS (700-1,000 μm) segment data (outer ring). In both panels, the inner blue ring signifies that data are relative to the ASCO. In the lower panel, the ASCOD-ppScleral data are surrounded by a mustard-colored outline to convey that they are measurements relative to the peripapillary scleral reference plane (Figure 3). All data are reported in right eye orientation. Within each ppSS segment and for ASCOD-ppScleral the 2 (or 3) steepest sectors (orange fonts) that were each significantly steeper (P < .05, Tukey test) than the 2, 3, 5, or 6 flattest sectors (blue fonts) are shown in 12 30-degree FoBMO sectors. ASCOD-ppScleral = anterior scleral canal opening depth relative to a 1,700-μm peripapillary scleral reference plane; FoBMO = fovea-to- Bruch's membrane opening distance; I = inferior; IT = inferior-temporal; N = nasal; NI = nasal-inferior; NS = nasal-superior; ppSS = peripapillary scleral slope; S = superior; SN = superior-nasal; ST = superior-temporal; T = temporal; TI = temporal-inferior; TS = temporal-superior.

• REPRODUCIBILITY: Interobserver segmentation reproducibility was assessed for all parameters within 8 OCT data sets from 8 study eyes independently segmented by 4 operators.

• STATISTICAL ANALYSIS: All statistical analyses were performed using SPSS version 24.0 softward (IBM, Armonk, New York) and R version 3.1.3 software (R Foundation, Vienna, Austria). Intraclass correlation coefficients between observers for each parameter were calculated by using a 2-way mixed model for agreement.[37] To assess the associations of demographic and ocular variables, as well other OCT parameters with the global ppSS and ASCOD-ppScleral, univariate and multivariate linear regression models were created as outlined in

Supplemental Figure 1. Variables or parameters that achieved a P significance <.2 in univariate analyses were entered into the multivariate regression, and variables achieving a P significance of <.05 and a variance inflation factor of <5 were considered significant.[38]

For sectoral ppSS and ASCOD-ppScleral, an analysis of variance (ANOVA) using a generalized estimating equation (GEE) model determine whether the parameters varied between sectors, followed by a post hoc Tukey test to identify significant pairwise differences. For each variable that was significantly associated with ppSS or ASCOD-ppScleral, additional GEE models were used to assess whether the association varied between FoBMO ONH sectors (Supplemental Figure 2). For the parameter ppSS, to account for the number of sectors and segments,

**TABLE 3.** Multivariate Analysis of Demographic, Ocular, and OCT Parameter Associations with Global OCT ppSclera Bowing Parameters by Linear Regression and the Significance of Sectoral Effects on Each Parameter by GEE

| Parameter | | Age | IOP | BMO/ASCO Area Ratio | ASCO Ovality | ASCO/BMO Offset | ppCT |
|---|---|---|---|---|---|---|---|
| ppSS (0-300) | Significance of coefficient[a] | **<0.001** | - | **<0.001** | **0.040** | **0.023** | **0.001** |
| | Standardized coefficient[a] | 0.24 | - | −0.35 | 0.10 | −0.12 | −0.20 |
| | Significance of sectoral effect[b] | **0.028** | - | 0.230 | **0.010** | **<0.001** | **0.038** |
| ppSS (300-700) | Significance of coefficient[a] | **<0.001** | - | **0.006** | **0.005** | - | **0.002** |
| | Standardized coefficient[a] | 0.34 | - | −0.15 | 0.15 | - | −0.18 |
| | Significance of sectoral effect[b] | **<0.001** | - | **<0.001** | 0.100 | - | **<0.001** |
| ppSS (700-1,000) | Significance of coefficient[a] | **<0.001** | - | **0.003** | **0.015** | **0.023** | - |
| | Standardized coefficient[a] | 0.45 | - | -0.15 | 0.12 | 0.11 | - |
| | Significance of sectoral effect[b] | **<0.001** | - | **0.005** | 0.112 | **0.029** | - |
| *ASCOD*-ppScleral | Significance of coefficient[a] | <0.001 | 0.039 | <0.001 | 0.007 | - | 0.006 |
| | Standardized coefficient[a] | 0.38 | 0.10 | −0.21 | 0.14 | - | −0.15 |
| | Significance of sectoral effect[b] | **0.015** | 0.085 | **<0.001** | **0.038** | - | **0.027** |

ppSS= peripapillary scleral slope; ASCO = anterior sclera canal opening; *ASCOD*-ppScleral = ASCO depth relative to a peripapillary scleral reference plane; BMO = Bruch's membrane opening; GEE = general estimation equation; IOP = intraocular pressure; OCT = optical coherence tomography; ppCT = peripapillary choroidal thickness.

Results are left blank for parameters not included in a given model for either global or sectoral effects analyses. *P*-values <0.05 were given in bold.

[a]Associations between each global parameter and each variable are presented as a standardized coefficient and significance as analyzed by multivariable linear regression.

[b]To assess whether the effects of each variable varied by sector, a GEE model was used for sectoral data.

and therefore the number of comparisons, the model included only variables for which 3 contiguous sector-segments achieved a $P < .05$ and a variance inflation factor of <5 (12 FoBMO sectors × 3 ppSS segments [0-300 μm, 300-700 μm, 700-1,000 μm] = 36 sector-segments total). For *ASCOD-ppScleral* (which was reported in 12 FoBMO sectors), the model required 2 contiguous FoBMO sectors to achieve significance by the same criteria for a variable to be included. The authors separately identified the subset of sectors (*ASCOD-ppScleral*) or sector-segments (ppSS) for which the P value in the multivariate analyses ($P < .05$) achieved significance after Bonferroni correction ($P < .00139$ [36 sector-segments]) for ppSS and ($P < .00416$ [12 sectors] for *ASCOD-ppScleral*).

# RESULTS

A TOTAL OF 362 EYES OF 362 SUBJECTS WERE STUDIED. DEMO-graphic and ocular data overall and by ethnicity have been previously reported[1,27,28] and are summarized in Table 1.

• PPSS: Mean global ppSS (0-300), ppSS (300-700), and ppSS (700-1,000) are reported in Table 2. The distribution of global ppSS at each ASCO distance (Figure 4) extended from modestly negative (inward bowing by convention) to substantially positive (outward bowing by convention). Overall and age-stratified sectoral ppSS values are reported

in Figure 5. Mean sectoral ppSS (0-300) differed between sectors ($P < .0001$, GEE ANOVA), ranging from 2.23 to 4.35, with the 2 steepest sectors (temporal and temporal-superior) each significantly steeper than the 2 flattest sectors (nasal-inferior and inferior-nasal; each comparison $P \leq .05$, Tukey test) (Figure 5). Mean sectoral ppSS (300-700) also differed between sectors ($P < .0001$, GEE ANOVA), ranging from 1.32 to 4.24 with the 3 steepest sectors (temporal, temporal-inferior, and inferior-temporal) each steeper than the 6 flattest sectors (superior-temporal, superior, superior-nasal, nasal-superior, nasal, and nasal-inferior) (Figure 5). Finally, mean sectoral ppSS (700-1,000) also differed between sectors ($P < .0001$, GEE ANOVA) ranging from 1.57 to 4.33, with the 2 steepest sectors (inferior and inferior-temporal) each steeper than the 6 flattest sectors (superior-temporal, superior, superior nasal, nasal-superior, nasal, and nasal inferior) (Figure 5).

Global ppSS for all 3 peripapillary scleral segments increased with age (standardized coefficient Beta = 0.24, 0.34, and 0.45, respectively; all $P < .001$) (Table 3). More modest effects were also significant for the BMO/ASCO area ratio, ASCO ovality, ASCO/BMO offset, and *ppCT* (Table 3). The sectoral effects of age, IOP, BMO/ASCO area ratio, ASCO ovality, ASCO/BMO offset, and *ppCT* are presented and compared in Figure 6 and Table 3.

• ASCOD-PPSCLERAL: Mean global *ASCOD-ppScleral* and its distribution by age are shown in Table 2 and Figure 4,
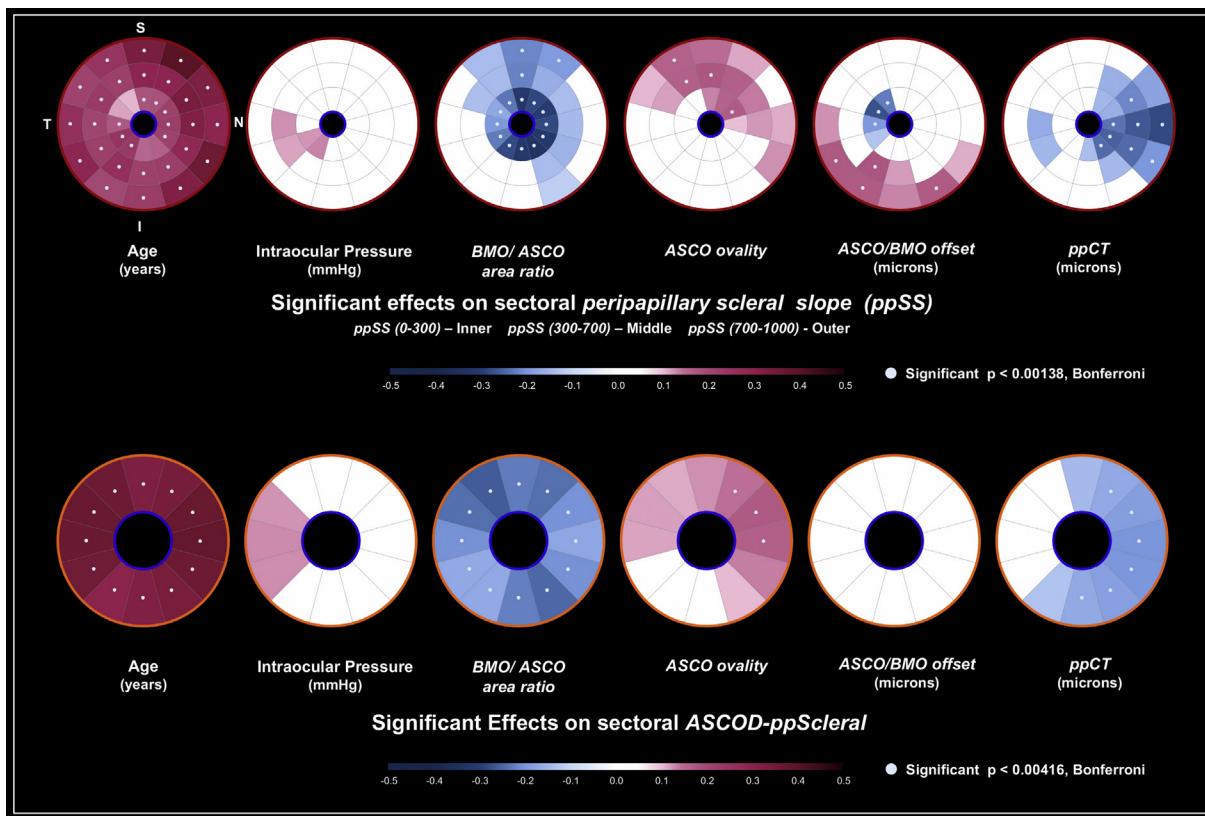
FIGURE 6. Significant sectoral demographic, ocular, and OCT parameter associations with the OCT peripapillary scleral bowing parameters by multivariate analysis. The strength of a linear relationship between each bowing parameter (ppSS above and ASCOD-ppScleral below) and each variable (age, intraocular pressure, BMO/ASCO area ratio, ASCO ovality, and ASCO/BMO offset) is depicted by the standardized regression coefficients for those sectors that achieved significance ($P \leq .05$, multivariate analysis [Methods and Supplemental Figure 2]). The color pink stands for a positive association and blue for a negative association. Because of the number of comparisons and to enhance clinical relevance, each significant variable was required to have achieved statistical significance within the multivariate analysis in at least 2 continuous sectors for ASCOD-ppScleral (12 sectors) or 3 contiguous sector segments for ppSS (36-sector segments). Thus, single sectoral associations are not reported. All data are reported in right eye orientation (upper left). Then the subset of sectors (ASCOD-ppScleral) or FoBMO sector-segments (ppSS) were identified separately that were significant within the multivariate analyses ($P < .05$) with P values that also achieved significance after Bonferroni correction ($P < .00139$ [36-sector segments] ppSS, and $P < .00416$ [12 sectors] ASCOD-ppScleral; white overlaid dots). ASCOD-ppScleral = anterior scleral canal opening depth relative to a 1,700-μm peripapillary scleral reference plane; BMO = Bruch's membrane opening; FoBMO = fovea-to-Bruch's membrane opening distance; OCT = optical coherence tomography; ppSS = peripapillary scleral slope.

respectively. Mean sectoral ASCOD-ppScleral differed between sectors ($P < .0001$, GEE ANOVA), ranging from 18.6 to 34.0 μm with the 2 steepest sectors (temporal-inferior and temporal) each significantly steeper than the 5 flattest sectors (superior-temporal, superior, superior-nasal, nasal-superior, and inferior) ($P \leq .05$, Tukey test) (Figure 5). By multivariate analysis, global ASCOD-ppScleral substantially increased with age (Beta = 0.38; $P < .001$), modestly increased with IOP and ASCO ovality, and modestly decreased with BMO/ASCO area ratio, and was modestly associated with decreasing ppCT (Table 3). Significant sectoral effects were present in all 12 sectors for age and BMO/ASCO area ratio and more localized for IOP (temporally), ASCO ovality (nasally), and ppCT, respectively (Figure 6).

• INTEROBSERVER REPRODUCIBILITY: Intraclass correlation coefficients showed moderate to excellent reproducibility for global and sectoral parameters (Supplemental Table 1).

## DISCUSSION

THIS STUDY INTRODUCES 2 NEW, 3D OCT PARAMETERS to characterize peripapillary scleral bowing, categorized as ppSS based on the peripapillary sclera and ASCOD-ppScleral based on the depth of ASCO relative to a peripapillary reference plane in a large cohort of healthy eyes. In so doing, the study lays a foundation
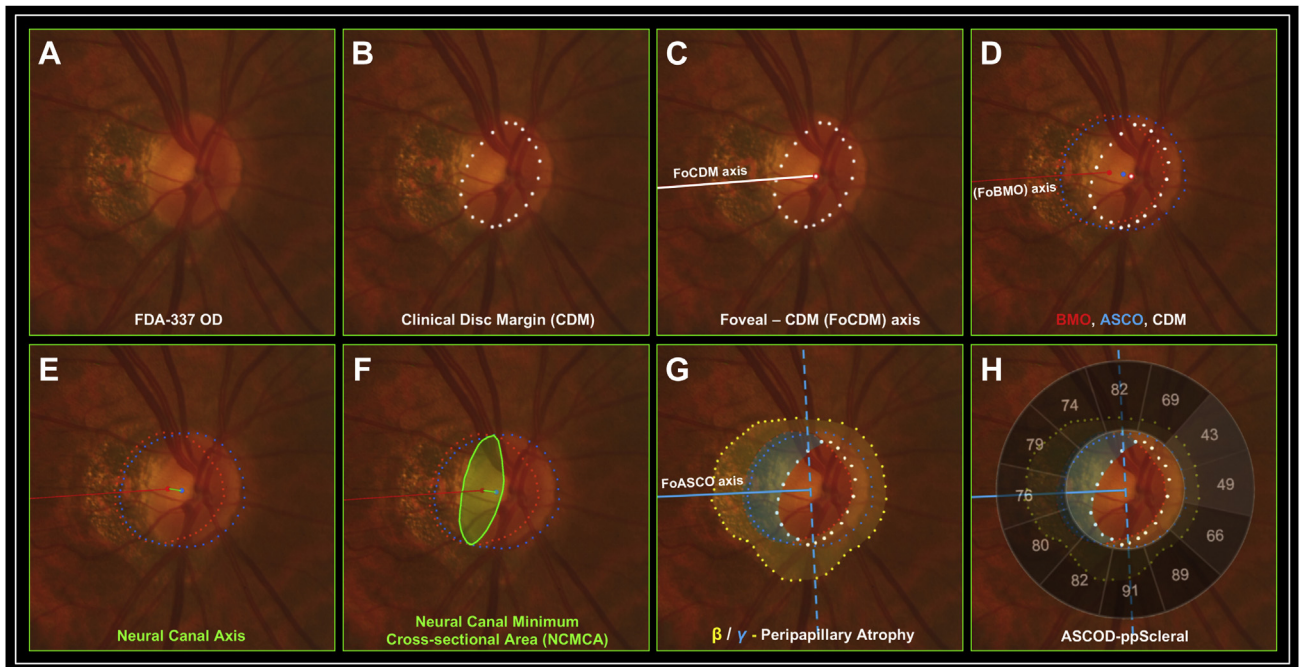
FIGURE 7. The authors predict that the ONH neural canal[1] and peripapillary scleral anatomy contribute to the clinical susceptibility of the ONH tissues to aging, peripapillary atrophy, glaucoma, and myopia and that OCT characterization of this anatomy will be required for these contributions to be identified. (A) Right eye of FDA337 (axial length: 25.10 mm; spherical equivalent: −5.5 diopter). (B) CDM is defined by the innermost hyper-reflective border of the ONH. (C) The FoCDM axis. (D) The CDM, BMO, the ASCO, and the FoBMO centroid axis projected onto the BMO plane. (E) The neural canal axes, defined by the vector connecting the BMO and ASCO centroids, are shown relative to the FoBMO axis for reference. (F) The NCMCA (as defined in a previous publication)[1] is smaller and more elliptical than the CDM, BMO, and the ASCO. (G) The beta (β) and gamma (γ) peripapillary atrophy relative to the FoASCO axis. (H) Peripapillary scleral bowing was quantified by *ASCOD-ppScleral* grey-scale sectors depict the percentile of the healthy eye distribution. Cross-sectional and longitudinal studies to determine whether increases in peripapillary scleral bowing underlie the increases in peripapillary atrophy seen in aging, glaucoma and myopia are required. ASCO = anterior scleral canal opening; *ASCOD-ppScleral* = anterior scleral canal opening depth relative to a 1,700-μm peripapillary scleral reference plane; BMO = Bruch's membrane opening; CDM = clinical disc margin; FoASCO = fovea-to-ASCO centroid; FoCDM = fovea-to-CDM centroid; NCMCA = neural canal minimum cross-sectional area; OCT = optical coherence tomography; ONH = optic nerve head.

for the incorporation of these ONH morphologic components into OCT-based strategies to clinically realize the phenotype and stage the ppScleral bowing[3] and posterior scleral remodeling[39–42] in aging, glaucoma, and myopia (Figure 7).[43–49] In healthy eyes, both peripapillary scleral bowing parameters reached substantial levels in a subset of eyes, dramatically increased with age and were independently associated with peripapillary choroidal thinning.

Peripapillary scleral bowing increased with age and was significantly associated with peripapillary choroidal thinning in 619 elderly (mean 60 years old) Chinese subjects, using a single horizontal B-scan.[3] This study replicates both of these findings, extends them to a different ethnic population that spans a much larger age range, and introduces a 3D characterization of peripapillary scleral bowing that includes sectoral measurements of peripapillary scleral slope and ASCO depth relative to a peripapillary scleral reference plane. This approach will allow peripapillary scleral bowing to be precisely mapped within individual eyes (Figure 7) in order to assess its contribution to ONH susceptibility in future cross-sectional and longitudinal studies.

The fact that peripapillary scleral bowing increased with age and was independently associated with peripapillary choroidal thinning (after accounting for age effects) in both studies suggests that it may mechanistically contribute to the increase in the prevalence of peripapillary atrophy with age[4–8] and in glaucoma.[5,9,10] Outward bowing of the peripapillary sclera and peripapillary atrophy are also hallmarks of the clinical appearance of the ONH in high myopia.[13,50–53] Age and high myopia are 2 of the most important risk factors for glaucoma at all levels of IOP, especially when it occurs at statistically normal levels of IOP.[54–56] Our findings support the broader concept that the presence of peripapillary

scleral bowing may increase the susceptibility of the ONH tissues to peripapillary choroidal atrophy and glaucoma in eyes of all ages and axial lengths.[13] These findings, therefore, suggest that cross-sectional and longitudinal studies to test these hypotheses may be indicated.[13]

The limitations of this study include the fact that in this and preceding papers[1,27,28] the ASCO was identified by projecting the immediate peripapillary scleral surface through the border tissues of Elschnig to the neural canal boundary (Figure 1). Unlike BMO, which is an anatomically identifiable structure in most nonmyopic eyes[57] by histology and by OCT[36,58,59] the ASCO is not an anatomically identifiable structure in either modality. However, although ASCO was estimated in this manner, the interoperator reproducibility of ASCO area and all related parameters were excellent. The clinical utility of the ONH parameters reported here is additionally limited by the fact that automated segmentation of the underlying anatomic landmarks is not yet possible, and manual segmentation by trained observers is required. However, the present authors believe that, if the clinical importance of the deep ONH anatomy of this study can be demonstrated, manual segmentations of that anatomy will provide training and testing data sets for the optimization of automated approaches.

Finally, although the use of manual segmentation limits the immediate clinical application of this work, the segmented anatomy and parameters generated here are also a strength of this study. Unsupervised deep learning algorithms,[60,61] which work with raw (unsegmented) OCT images, may eventually incorporate the anatomy of this study into strategies for detecting glaucoma and its progression without segmenting any ONH anatomic targets. However, supervised machine learning algorithms,[62,63] which require segmented anatomy and/or parameterization, may also be required to inform our understanding of disease staging and mechanisms. Structurally distinguishing and staging the effects of aging, glaucoma, and myopia on the ONH tissues is important because it may provide insight into their respective underlying pathophysiologic mechanisms and inform future therapeutic interventions. The authors believe that manually segmented anatomy will be a required component of efforts to move the field toward disease staging and automated interpretations of OCT anatomy.

In summary, this study developed a 3D, OCT-based strategy to clinically characterize ppScleral bowing and used it to study non-highly myopic eyes that included up to −6 D of spherical equivalent refractive error. The study found that ppScleral bowing can be substantial in non-highly myopic healthy eyes, increased dramatically with age, and was independently associated with peripapillary choroidal thinning. Our OCT parameters provide a foundation for cross-sectional and longitudinal studies of this anatomy in aging, glaucoma, and high myopia and in eyes with optic disc tilt, torsion, and peripapillary atrophy.

# REFERENCES

1. Hong S, Yang H, Gardiner SK, et al. OCT-detected optic nerve head neural canal direction, obliqueness and minimum cross-sectional area in healthy eyes. *Am J Ophthalmol* 2019; 208:185–205.
2. Downs JC, Yang H, Girkin C, et al. Three-dimensional histomorphometry of the normal and early glaucomatous monkey optic nerve head: neural canal and subarachnoid space architecture. *Invest Ophthalmol Vis Sci* 2007;48(7): 3195–3208.
3. Tun TA, Wang X, Baskaran M, et al. Variation of Peripapillary Scleral Shape With Age. *Invest Ophthalmol Vis Sci* 2019; 60(10):3275–3282.
4. Burgoyne CF, Downs JC. Premise and prediction-how optic nerve head biomechanics underlies the susceptibility and clinical behavior of the aged optic nerve head. *J Glaucoma* 2008;17(4):318–328.
5. Jonas JB, Fernandez MC, Naumann GO. Parapapillary atrophy and retinal vessel diameter in nonglaucomatous optic nerve damage. *Invest Ophthalmol Vis Sci* 1991;32(11): 2942–2947.

6. Wang Y, Xu L, Zhang L, Yang H, Ma Y, Jonas JB. Peripapillary atrophy in elderly Chinese in rural and urban Beijing. *Eye (Lond)* 2008;22(2):261–266.

7. Rockwood EJ, Anderson DR. Acquired peripapillary changes and progression in glaucoma. *Graefes Arch Clin Exp Ophthalmol* 1988;226(6):510–515.

8. Zhang Q, Wang YX, Wei WB, Xu L, Jonas JB. Parapapillary beta zone and gamma zone in a healthy population: the Beijing Eye Study 2011. *Invest Ophthalmol Vis Sci* 2018;59(8):3320–3329.

9. Jonas JB. Clinical implications of peripapillary atrophy in glaucoma. *Curr Opin Ophthalmol* 2005;16(2):84–88.

10. Buus DR, Anderson DR. Peripapillary crescents and halos in normal-tension glaucoma and ocular hypertension. *Ophthalmology* 1989;96(1):16–19.

11. Burgoyne CF, Downs JC, Bellezza AJ, Suh JK, Hart RT. The optic nerve head as a biomechanical structure: a new paradigm for understanding the role of IOP–related stress and strain in the pathophysiology of glaucomatous optic nerve head damage. *Prog Retin Eye Res* 2005;24(1):39–73.

12. Burgoyne CF. A biomechanical paradigm for axonal insult within the optic nerve head in aging and glaucoma. *Exp Eye Res* 2011;93(2):120–132.

13. Kim EK, Park H-YL, Park CK. Posterior scleral deformations around optic disc are associated with visual field damage in open-angle glaucoma patients with myopia. *PLoS One* 2019;14(3):e0213714.

14. Chen JY, Le A, De Andrade LM, Goseki T, Demer JL. Compression of the choroid by horizontal duction. *Invest Ophthalmol Vis Sci* 2019;60(13):4285–4291.

15. Suh SY, Le A, Shin A, Park J, Demer JL. Progressive deformation of the optic nerve head and peripapillary structures by graded horizontal duction. *Invest Ophthalmol Vis Sci* 2017;58(12):5015–5021.

16. Langham M. The temporal relation between intraocular pressure and loss of vision in chronic simple glaucoma. *Glaucoma* 1980;2(4):427–435.

17. Pijanka JK, Coudrillier B, Ziegler K, et al. Quantitative mapping of collagen fiber orientation in non-glaucoma and glaucoma posterior human sclerae. *Invest Ophthalmol Vis Sci* 2012;53(9):5258–5270.

18. Coudrillier B, Pijanka J, Jefferys J, et al. Collagen structure and mechanical properties of the human sclera: analysis for the effects of age. *J Biomech Eng* 2015;137(4):041006.

19. Hernandez MR, Luo XX, Igoe F, Neufeld AH. Extracellular matrix of the human lamina cribrosa. *Am J Ophthalmol* 1987;104(6):567–576.

20. Sigal IA, Flanagan JG, Tertinegg I, Ethier CR. Finite element modeling of optic nerve head biomechanics. *Invest Ophthalmol Vis Sci* 2004;45(12):4378–4387.

21. Sigal IA, Yang H, Roberts MD, et al. IOP-induced lamina cribrosa deformation and scleral canal expansion: independent or related? *Invest Ophthalmol Vis Sci* 2011;52(12):9023–9032.

22. Burgoyne CF, Downs JC, Bellezza AJ, Hart RT. Three-dimensional reconstruction of normal and early glaucoma monkey optic nerve head connective tissues. *Invest Ophthalmol Vis Sci* 2004;45(12):4388–4399.

23. Yang H, Downs JC, Bellezza A, Thompson H, Burgoyne CF. 3-D histomorphometry of the normal and early glaucomatous monkey optic nerve head: prelaminar neural tissues and cupping. *Invest Ophthalmol Vis Sci* 2007;48(11):5068–5084.

24. Sugiyama K, Cioffi GA, Bacon DR, Van Buskirk EM. Optic nerve and peripapillary choroidal microvasculature in the primate. *J Glaucoma* 1994;3(Suppl 1):S45–S54.

25. Hayreh SS, Revie IH, Edwards J. Vasogenic origin of visual field defects and optic nerve changes in glaucoma. *Br J Ophthalmol* 1970;54(7):461–472.

26. Hayreh SS. Blood supply of the optic nerve head and its role in optic atrophy, glaucoma, and oedema of the optic disc. *Br J Ophthalmol* 1969;53(11):721–748.

27. Yang H, Luo H, Gardiner SK, et al. Factors influencing optical coherence tomography peripapillary choroidal thickness: a multicenter study. *Invest Ophthalmol Vis Sci* 2019;60(2):795–806.

28. Luo H, Yang H, Gardiner SK, et al. Factors influencing central lamina cribrosa depth: a multicenter study. *Invest Ophthalmol Vis Sci* 2018;59(6):2357–2370.

29. Chauhan BC, Danthurebandara VM, Sharpe GP, et al. Bruch's membrane opening minimum rim width and retinal nerve fiber layer thickness in a normal white population: a multicenter study. *Ophthalmology* 2015;122(9):1786–1794.

30. United States Census. Statistical Abstract of The United States: 2012. Available at: https://www.census.gov/library/publications/2011/compendia/statab/131ed.html. Accessed May 12, 2020.

31. Burgoyne C. The morphological difference between glaucoma and other optic neuropathies. *J Neuroophthalmol* 2015;35(Suppl 1):S8–S21.

32. Chauhan BC, Burgoyne CF. From clinical examination of the optic disc to clinical assessment of the optic nerve head: a paradigm change. *Am J Ophthalmol* 2013;156(2):218–227.

33. He L, Ren R, Yang H, et al. Anatomic vs. acquired image frame discordance in spectral domain optical coherence tomography minimum rim measurements. *PLoS One* 2014;9(3):e92225.

34. Spaide RF, Koizumi H, Pozzoni MC. Enhanced depth imaging spectral-domain optical coherence tomography. *Am J Ophthalmol* 2008;146(4):496–500.

35. Fortune B, Reynaud J, Hardin C, Wang L, Sigal IA, Burgoyne CF. Experimental glaucoma causes optic nerve head neural rim tissue compression: a potentially important mechanism of axon injury. *Invest Ophthalmol Vis Sci* 2016;57(10):4403–4411.

36. Strouthidis NG, Yang H, Fortune B, Downs JC, Burgoyne CF. Detection of optic nerve head neural canal opening within histomorphometric and spectral domain optical coherence tomography data sets. *Invest Ophthalmol Vis Sci* 2009;50(1):214–223.

37. Koo T, Li MY. Abstracts of the Scientific Sessions from the WFC'S 12th Biennial Congress Proceedings. Durban, South Africa, April 10–13, 2013. *J Chiropr Med* 2013;12(2):92–142.

38. Craney TA, Surles JG. Model-dependent variance inflation factor cutoff values. *Qual Engr* 2002;14:391–403.

39. Kim YC, Jung KI, Park HL, Park CK. Three-dimensional evaluation of posterior pole and optic nerve head in myopes with glaucoma. *Sci Rep* 2017;7(1):18001.

40. Kim YC, Jung Y, Park HL, Park CK. the location of the deepest point of the eyeball determines the optic disc configuration. *Sci Rep* 2017;7(1):5881.

41. Kim YC, Moon JS, Park HL, Park CK. Three dimensional evaluation of posterior pole and optic nerve head in tilted disc. *Sci Rep* 2018;8(1):1121.

42. Moriyama M, Ohno-Matsui K, Hayashi K, et al. Topographic analyses of shape of eyes with pathologic myopia by high-resolution three-dimensional magnetic resonance imaging. *Ophthalmology* 2011;118(8):1626–1637.

43. Witmer MT, Margo CE, Drucker M. Tilted optic disks. *Surv Ophthalmol* 2010;55(5):403–428.

44. Lee KM, Lee EJ, Kim TW. Lamina cribrosa configuration in tilted optic discs with different tilt axes: a new hypothesis regarding optic disc tilt and torsion. *Invest Ophthalmol Vis Sci* 2015;56(5):2958–2967.

45. Choi JA, Park HY, Shin HY, Park CK. Optic disc tilt direction determines the location of initial glaucomatous damage. *Invest Ophthalmol Vis Sci* 2014;55(8):4991–4998.

46. Kim TW, Kim M, Weinreb RN, Woo SJ, Park KH, Hwang JM. Optic disc change with incipient myopia of childhood. *Ophthalmology* 2012;119(1):21–26.

47. Sung MS, Kang YS, Heo H, Park SW. Characteristics of optic disc rotation in myopic eyes. *Ophthalmology* 2016;123(2):400–407.

48. Sung MS, Kang YS, Heo H, Park SW. Optic disc rotation as a clue for predicting visual field progression in myopic normal-tension glaucoma. *Ophthalmology* 2016;123(7):1484–1493.

49. Marsh-Tootle WL, Harb E, Hou W, et al. Optic nerve tilt, crescent, ovality, and torsion in a multi-ethnic cohort of young adults with and without myopia. *Invest Ophthalmol Vis Sci* 2017;58(7):3158–3171.

50. Curtin BJ, Iwamoto T, Renaldo DP. Normal and staphylomatous sclera of high myopia: an electron microscopic study. *Arch Ophthalmol* 1979;97(5):912–915.

51. Ohno-Matsui K, Jonas JB. Posterior staphyloma in pathologic myopia. *Prog Retin Eye Res* 2019;70:99–109.

52. Jonas JB, Gusek GC, Naumann GO. Optic disk morphometry in high myopia. *Graefes Arch Clin Exp Ophthalmol* 1988; 226(6):587–590.

53. Xu L, Li Y, Wang S, Wang Y, Wang Y, Jonas JB. Characteristics of highly myopic eyes: the Beijing Eye Study. *Ophthalmology* 2007;114(1):121–126.

54. Marcus MW, de Vries MM, Junoy Montolio FG, Jansonius NM. Myopia as a risk factor for open-angle glaucoma: a systematic review and meta-analysis. *Ophthalmology* 2011;118(10):1989–1994.

55. Leske MC, Connell AM, Wu SY, Hyman LG, Schachat AP. Risk factors for open-angle glaucoma. The Barbados Eye Study. *Arch Ophthalmol* 1995;113(7):918–924.

56. Drance S, Anderson DR, Schulzer M. Risk factors for progression of visual field abnormalities in normal-tension glaucoma. *Am J Ophthalmol* 2001;131(6):699–708.

57. Strouthidis NG, Yang H, Downs JC, Burgoyne CF. Comparison of clinical and three-dimensional histomorphometric optic disc margin anatomy. *Invest Ophthalmol Vis Sci* 2009; 50(5):2165–2174.

58. Strouthidis NG, Yang H, Reynaud JF, et al. Comparison of clinical and spectral domain optical coherence tomography optic disc margin anatomy. *Invest Ophthalmol Vis Sci* 2009; 50(10):4709–4718.

59. Strouthidis NG, Grimm J, Williams GA, Cull GA, Wilson DJ, Burgoyne CF. A comparison of optic nerve head morphology viewed by spectral domain optical coherence tomography and by serial histology. *Invest Ophthalmol Vis Sci* 2010;51(3):1464–1474.

60. Christopher M, Belghith A, Weinreb RN, et al. Retinal nerve fiber layer features identified by unsupervised machine learning on optical coherence tomography scans predict glaucoma progression. *Invest Ophthalmol Vis Sci* 2018;59(7): 2748–2756.

61. Maetschke S, Antony B, Ishikawa H, Wollstein G, Schuman J, Garnavi R. A feature agnostic approach for glaucoma detection in OCT volumes. *PLoS One* 2019;14(7): e0219126.

62. Song Y, Ishikawa H, Wu M, et al. Clinical prediction performance of glaucoma progression using a 2-dimensional continuous-time hidden Markov model with structural and functional measurements. *Ophthalmology* 2018;125(9): 1354–1361.

63. Wang P, Shen J, Chang R, et al. Machine learning models for diagnosing glaucoma from retinal nerve fiber layer thickness maps. *Ophthalmology Glaucoma* 2019;2(6):422–428.